대한기계학회 2001년도 춘계학술대회논문집 A pp. 102~107 KSME 01S007

Analysis of Propagating Crack Along Interface of Isotropic-Orthotropic Bimaterial by Photoelastic Experiment

K.H., Lee* , A., Shukla**, V., Parameswaran**, V., Chalivendra** , J.S., Hawong***

Key Words : Static and Dynamic Stress Intensity Factor, Interface Crack, Isotropic-Orthotropic Bimaterial, Energy Release Rate

Abstract

Interfacial cracks between an isotropic and orthotropic material, subjected to static far field tensile loading are analyzed using the technique of photoelasticity. The fracrure parameters are extracted from the full-field isochromatic data and the same are compared with that obtained using boundary collocation method. Dynamic Photoelasticity combined with high-speed digital photography is employed for capturing the isochromatics in the case of propagating interfacial cracks. The normalized stress intensity factors for static crack is greater when α=90° (fibers perpendicular to the interface) than when α=0° (fiber parallel to the interface) and those when α=90° are similar to ones of isotropic material. The dynamic stress intensity factors for interfacial propagating crack are greater when α=0° than α=90°. The relationship between complex dynamic stress intensity factor $|K_D|$ and crack speed c is similar to that for isotropic homogeneous materials, the rate of increase of energy release rate G or $|K_D|$ with crack speed is not as drastic as that reported for homogeneous materials.

1. Introduction

Interface cracks in view of their importance in numerous applications have received considerable attention in the literature devoted to fracture mechanics[1-3]. Gdoutos[4] and Lu[5] had determined the static stress intensity factor for bimaterial specimens using photoelatiscity. Lambrous and Rosakis[6] and Kavaturu and Shukla[7] have independently proposed fracture criteria for dynamic propagating interfacial cracks. While the static and dynamic fracture of isotropic-orthotropic bimaterial fracture has extensively been considered theoretically, the experimental investigations of this problem is rather limited. In the present study, a detailed experimental investigation is conducted to determine stress intensity factor and energy release rate associated with stationary and propagating cracks along the interface of isotropic-orthotropic bimaterial. High-speed photography coupled with photoelasticity is used to capture the isochromatic fringe pattern.

* Sangju National University
** University of Rhode Island
*** Yeoungnam University

2. Stress and Displacement Fields

The oscillatory stress fields[3] with odd power series (n=1,3,5,...) for the material above the interface (the isotropic material) can be represented as

$$\sigma_{xn}=\sum_{n=odd}\frac{K_n^o}{2\sqrt{2\pi D\cosh\varepsilon\pi}}\Big\{-(1+2\beta_l^2-\beta_s^2)[e^{\varepsilon(\pi-\theta_l)}\,\overline{A}\cos(\varepsilon\ln\frac{r_l}{2a}+\frac{n-2}{2}\theta_l)-e^{-\varepsilon(\pi-\theta_l)}\,A\cos(\varepsilon\ln\frac{r_l}{2a}-\frac{n-2}{2}\theta_l)]r_l^{\frac{n-2}{2}}-2\beta_s[e^{\varepsilon(\pi-\theta_s)}\,\overline{B}\cos(\varepsilon\ln\frac{r_s}{2a}+\frac{n-2}{2}\theta_s)+e^{-\varepsilon(\pi-\theta_s)}\,B\cos(\varepsilon\ln\frac{r_s}{2a}-\frac{n-2}{2}\theta_s)]r_s^{\frac{n-2}{2}}\Big\}+\sum_{n=odd}\frac{K_n^*}{2\sqrt{2\pi D\cosh\varepsilon\pi}}\Big\{(1+2\beta_l^2-\beta_s^2)[e^{\varepsilon(\pi-\theta_l)}\,\overline{A}\sin(\varepsilon\ln\frac{r_l}{2a}+\frac{n-2}{2}\theta_l)-e^{-\varepsilon(\pi-\theta_l)}\,A\sin(\varepsilon\ln\frac{r_l}{2a}-\frac{n-2}{2}\theta_l)]r_l^{\frac{n-2}{2}}+2\beta_s[e^{\varepsilon(\pi-\theta_s)}\,\overline{B}\sin(\varepsilon\ln\frac{r_s}{2a}+\frac{n-2}{2}\theta_s)+e^{-\varepsilon(\pi-\theta_s)}\,B\sin(\varepsilon\ln\frac{r_s}{2a}-\frac{n-2}{2}\theta_s)]r_s^{\frac{n-2}{2}}\Big\} \tag{1}$$

$$\sigma_{yn}=\sum_{n=odd}\frac{K_n^o}{2\sqrt{2\pi}D\cosh\varepsilon\pi}\Big\{(1+\beta_s^2)[e^{\varepsilon(\pi-\theta_l)}\ \bar{A}\cos(\varepsilon\ln\frac{r_l}{2a}+\frac{n-2}{2}\theta_l)-e^{-\varepsilon(\pi-\theta_l)}\ A\cos(\varepsilon\ln\frac{r_l}{2a}-\frac{n-2}{2}\theta_l)]r_l^{\frac{n-2}{2}}$$
$$+2\beta_s[e^{\varepsilon(\pi-\theta_s)}\ \bar{B}\cos(\varepsilon\ln\frac{r_s}{2a}+\frac{n-2}{2}\theta_s)+e^{-\varepsilon(\pi-\theta_s)}\ B\cos(\varepsilon\ln\frac{r_s}{2a}-\frac{n-2}{2}\theta_s)]r_s^{\frac{n-2}{2}}\Big\}$$
$$+\sum_{n=odd}\frac{K_n^*}{2\sqrt{2\pi}D\cosh\varepsilon\pi}\Big\{-(1+\beta_s^2)[e^{\varepsilon(\pi-\theta_l)}\ \bar{A}\sin(\varepsilon\ln\frac{r_l}{2a}+\frac{n-2}{2}\theta_l)-e^{-\varepsilon(\pi-\theta_l)}\ A\sin(\varepsilon\ln\frac{r_l}{2a}-\frac{n-2}{2}\theta_l)]r_l^{\frac{n-2}{2}}$$
$$-2\beta_s[e^{\varepsilon(\pi-\theta_s)}\ \bar{B}\sin(\varepsilon\ln\frac{r_s}{2a}+\frac{n-2}{2}\theta_s)+e^{-\varepsilon(\pi-\theta_s)}\ B\sin(\varepsilon\ln\frac{r_s}{2a}-\frac{n-2}{2}\theta_s)]r_s^{\frac{n-2}{2}}\Big\} \tag{2}$$

$$\tau_{xyn}=\sum_{n=odd}\frac{K_n^o}{2\sqrt{2\pi}D\cosh\varepsilon\pi}\Big\{2\beta_l[e^{\varepsilon(\pi-\theta_l)}\ \bar{A}\sin(\varepsilon\ln r_l+\frac{n-2}{2}\theta_l)+e^{-\varepsilon(\pi-\theta_l)}\ A\sin(\varepsilon\ln r_l-\frac{n-2}{2}\theta_l)]r_l^{\frac{n-2}{2}}$$
$$+(1+\beta_s^2)[e^{\varepsilon(\pi-\theta_s)}\ \bar{B}\sin(\varepsilon\ln r_s+\frac{n-2}{2}\theta_s)-e^{-\varepsilon(\pi-\theta_s)}\ B\sin(\varepsilon\ln r_s-\frac{n-2}{2}\theta_s)]r_s^{\frac{n-2}{2}}\Big\}$$
$$+\sum_{n=odd}\frac{K_n^*}{2\sqrt{2\pi}D\cosh\varepsilon\pi}\Big\{2\beta_l[e^{\varepsilon(\pi-\theta_l)}\ \bar{A}\cos(\varepsilon\ln\frac{r_l}{2a}+\frac{n-2}{2}\theta_l)+e^{-\varepsilon(\pi-\theta_l)}\ A\cos(\varepsilon\ln\frac{r_l}{2a}-\frac{n-2}{2}\theta_l)]r_l^{\frac{n-2}{2}}$$
$$+(1+\beta_s^2)[e^{\varepsilon(\pi-\theta_s)}\ \bar{B}\cos(\varepsilon\ln\frac{r_s}{2a}+\frac{n-2}{2}\theta_s)-e^{-\varepsilon(\pi-\theta_s)}\ B\cos(\varepsilon\ln\frac{r_s}{2a}-\frac{n-2}{2}\theta_s)]r_s^{\frac{n-2}{2}}\Big\} \tag{3}$$

Where $n>0$, n=odd

$A=2\beta_s\eta+(1+\beta_s^2)$, $\bar{A}=2\beta_s\eta-(1+\beta_s^2)$

$B=2\beta_l+(1+\beta_s^2)\eta$, $\bar{B}=2\beta_l-(1+\beta_s^2)\eta$

Oscillatory displacement fields[3] with odd power series (n=1,3,5,... ,) can be represented as

$$u_{xn}=\sum_{n=odd}\frac{K_n^o}{\sqrt{2\pi}(n^2+4\varepsilon^2)\mu D\cosh\varepsilon\pi}$$
$$\Big\{-e^{\varepsilon(\pi-\theta_l)}\ \bar{A}[n\cos(\varepsilon\ln\frac{r_l}{2a}+\frac{n}{2}\theta_l)+2\varepsilon\sin(\varepsilon\ln\frac{r_l}{2a}+\frac{n}{2}\theta_l)]r_l^{\frac{n}{2}}$$
$$+e^{-\varepsilon(\pi-\theta_l)}A[n\cos(\varepsilon\ln\frac{r_l}{2a}-\frac{n}{2}\theta_l)+2\varepsilon\sin(\varepsilon\ln\frac{r_l}{2a}-\frac{n}{2}\theta_l)]r_l^{\frac{n}{2}}$$
$$-e^{\varepsilon(\pi-\theta_s)}\beta_s\bar{B}[n\cos(\varepsilon\ln\frac{r_s}{2a}+\frac{n}{2}\theta_s)+2\varepsilon\sin(\varepsilon\ln\frac{r_s}{2a}+\frac{n}{2}\theta_s)]r_s^{\frac{n}{2}}$$
$$-e^{-\varepsilon(\pi-\theta_s)}\beta_sB[n\cos(\varepsilon\ln\frac{r_s}{2a}-\frac{n}{2}\theta_s)+2\varepsilon\sin(\varepsilon\ln\frac{r_s}{2a}-\frac{n}{2}\theta_s)]r_s^{\frac{n}{2}}\Big\}$$
$$+\sum_{n=odd}\frac{K_n^*}{\sqrt{2\pi}(n^2+4\varepsilon^2)\mu D\cosh\varepsilon\pi}$$
$$\Big\{e^{\varepsilon(\pi-\theta_l)}\ \bar{A}[n\sin(\varepsilon\ln\frac{r_l}{2a}+\frac{n}{2}\theta_l)-2\varepsilon\cos(\varepsilon\ln\frac{r_l}{2a}+\frac{n}{2}\theta_l)]r_l^{\frac{n}{2}}$$
$$-e^{-\varepsilon(\pi-\theta_l)}A[n\sin(\varepsilon\ln\frac{r_l}{2a}-\frac{n}{2}\theta_l)-2\varepsilon\cos(\varepsilon\ln\frac{r_l}{2a}-\frac{n}{2}\theta_l)]r_l^{\frac{n}{2}}$$
$$+e^{\varepsilon(\pi-\theta_s)}\beta_s\bar{B}[n\sin(\varepsilon\ln\frac{r_s}{2a}+\frac{n}{2}\theta_s)-2\varepsilon\cos(\varepsilon\ln\frac{r_s}{2a}+\frac{n}{2}\theta_s)]r_s^{\frac{n}{2}}$$
$$+e^{-\varepsilon(\pi-\theta_s)}\beta_sB[n\sin(\varepsilon\ln\frac{r_s}{2a}-\frac{n}{2}\theta_s)-2\varepsilon\cos(\varepsilon\ln\frac{r_s}{2a}-\frac{n}{2}\theta_s)]r_s^{\frac{n}{2}}\Big\} \tag{4}$$

$$u_{yn}=\sum_{n=odd}\frac{K_n^o}{\sqrt{2\pi}\ (n^2+4\varepsilon^2)\mu D\cosh\varepsilon\pi}$$
$$\Big\{e^{\varepsilon(\pi-\theta_l)}\ \beta_l\bar{A}[n\sin(\varepsilon\ln\frac{r_l}{2a}+\frac{n}{2}\theta_l)-2\varepsilon\cos(\varepsilon\ln\frac{r_l}{2a}+\frac{n}{2}\theta_l)]r_l^{\frac{n}{2}}$$
$$+e^{-\varepsilon(\pi-\theta_l)}\beta_lA[n\sin(\varepsilon\ln\frac{r_l}{2a}-\frac{n}{2}\theta_l)-2\varepsilon\cos(\varepsilon\ln\frac{r_l}{2a}-\frac{n}{2}\theta_l)]r_l^{\frac{n}{2}}$$
$$+e^{\varepsilon(\pi-\theta_s)}\bar{B}[n\sin(\varepsilon\ln\frac{r_s}{2a}+\frac{n}{2}\theta_s)-2\varepsilon\cos(\varepsilon\ln\frac{r_s}{2a}+\frac{n}{2}\theta_s)]r_s^{\frac{n}{2}}$$
$$-e^{-\varepsilon(\pi-\theta_s)}B[n\sin(\varepsilon\ln\frac{r_s}{2a}-\frac{n}{2}\theta_s)-2\varepsilon\cos(\varepsilon\ln\frac{r_s}{2a}-\frac{n}{2}\theta_s)]r_s^{\frac{n}{2}}\Big\}$$
$$+\sum_{n=odd}\frac{K_n^*}{\sqrt{2\pi}(n^2+4\varepsilon^2)\mu D\cosh\varepsilon\pi}$$
$$\Big\{e^{\varepsilon(\pi-\theta_l)}\beta_l\bar{A}[n\cos(\varepsilon\ln\frac{r_l}{2a}+\frac{n}{2}\theta_l)+2\varepsilon\sin(\varepsilon\ln\frac{r_l}{2a}+\frac{n}{2}\theta_l)]r_l^{\frac{n}{2}}$$
$$+e^{-\varepsilon(\pi-\theta_l)}\beta_lA[n\cos(\varepsilon\ln\frac{r_l}{2a}-\frac{n}{2}\theta_l)+2\varepsilon\sin(\varepsilon\ln\frac{r_l}{2a}-\frac{n}{2}\theta_l)]r_l^{\frac{n}{2}}$$
$$+e^{\varepsilon(\pi-\theta_s)}\bar{B}[n\cos(\varepsilon\ln\frac{r_s}{2a}+\frac{n}{2}\theta_s)+2\varepsilon\sin(\varepsilon\ln\frac{r_s}{2a}+\frac{n}{2}\theta_s)]r_s^{\frac{n}{2}}$$
$$-e^{-\varepsilon(\pi-\theta_s)}B[n\cos(\varepsilon\ln\frac{r_s}{2a}-\frac{n}{2}\theta_s)+2\varepsilon\sin(\varepsilon\ln\frac{r_s}{2a}-\frac{n}{2}\theta_s)]r_s^{\frac{n}{2}}\Big\} \tag{5}$$

where $n>0$, n=odd. When n=1, eqs (1) ~(5) are stress and displacement fields around the propagating interfacial crack tip. Thus, K_1^o and K_1^* are stress intensity factors K_I and K_{II}. For far field stress σ_y^∞ and τ_{xy}^∞ at infinity, the stress intensity factors K_I and K_{II} are given as

$$K_I+iK_{II}=\sqrt{\pi a}(1+2i\varepsilon)\ (\sigma_y^\infty+i\frac{1}{\eta}\tau_{xy}^\infty) \tag{6}$$

The stress and displacements of eq.(1) ~eq.(5) can be represented as

$$\sigma_{ij}=\sum_{n=1}^{\infty}(A_n^oH_{ijn}^o+A_n^*H_{ijn}^*),\ u_i=\sum_{n=1}^{\infty}(A_n^oU_{in}^o+A_n^*U_{in}^*) \tag{7}$$

and the energy release rate is given by

$$G=\frac{(K_I^2+K_{II}^2)h_{21}}{4\cosh^2(\varepsilon\pi)} \tag{8}$$

where $A_n^o=\frac{K_n^o}{\sqrt{2\pi}}a^{n/2-1}$, $A_n^*=\frac{K_n^*}{\sqrt{2\pi}}a^{n/2-1}$

$\varepsilon=\frac{1}{2\pi}\ln\frac{1-\beta}{1+\beta}$, $\beta=\frac{h_{11}}{\sqrt{h_{12}h_{21}}}$

$h_{11}=(l_{11})_1-(l_{11})_2$, $h_{12}=(l_{12})_1+(l_{12})_2$

$h_{21}=(l_{21})_1+(l_{21})_2$, $\eta=(h_{21}/h_{12})^{1/2}$

$(l_{11})_1=\left\{\frac{2\beta_l\beta_s-(1+\beta_s^2)}{\mu D_1}\right\}$, $(l_{12})_1=\left\{\frac{\beta_s(1-\beta_s^2)}{\mu D_1}\right\}$

$(l_{21})_1=\left\{\frac{\beta_l(1-\beta_s^2)}{\mu D_1}\right\}$, $(l_{11})_2=\frac{p_s\alpha_l-p_l\alpha_s}{D_2}=\frac{q_s-q_l}{\alpha_s-\alpha_l}$

$(l_{12})_2=\frac{(1+M_a)(p_l-p_s)}{D_2}$, $(l_{21})_2=\frac{\alpha_sq_l-\alpha_lq_s}{D_2}$

$D_1=[4\beta_l\beta_s-(1+\beta_s^2)^2]$, $D_2=(1+M_a)(\alpha_s-\alpha_l)$

and $2a$ is crack length, the c, c_l and c_s are the crack propagation velocity, longitudinal and shear wave velocity for material 1(isotropic material) respectively. Meanwhile, the p_l, p_s, q_l, q_s, α_l, α_s, M_a and the fields for the material below the interface (the orthotropic material) are given in reference[3].

3. The Determination of Stress Intensity Factors by Boundary Collocation.

The bimaterial model which was used in this study is shown in Fig. 1 with the traction T_y applied on upper and lower boundaries. In the figure $\tau_{xy}=0$ on $\overline{AB}$, $T_y=\sigma$ on $\overline{BC}$, $\tau_{xy}=0$, $u_x=0$ on $\overline{CD}$, $T_y=\sigma$ on $\overline{DA}$. Since the loading, material and geometry are symmetric about vertical axis, only one half (right) of the plate is considered. The total number of the selected points along the boundary are 120 (40 along AB, 20 along BC, 40 along CD, 20 along DA). H^o_{ijn}, H^*_{ijn}, U^o_{xn} and U^*_{xn} can be obtained from boundary collocation points and material properties. The σ_{yn} and u_{xn} also are known from the boundary collocation points. Thus, A^o_n and A^*_n, which are unknown values, can be obtained from eq.(7). Therefore, the K^o_1 and K^*_1, which are K_I and K_{II}, respectively, can be obtained from A^o_n and A^*_n. Equation 7 is expanded for n=1,3,5,...,59 thus giving us 60 unknown coefficients: $A^o_1,\ldots,A^o_{59}$ and $A^*_1,\ldots,A^*_{59}$. When the boundary conditions, material properties and coordinates r,θ of the selected boundary are substituted into the general stress and displacement fields, 120 simultaneous equations with unknown coefficients A^o_n, A^*_n are constructed. The solutions, which satisfy the boundary conditions, are obtained by using least squares method.

If the external traction and elastic properties are symmetric about x-axis, τ_{xy} is zero along the x-axis. Under these circumstances, only the term A^o_n which is related to stress intensity factor K_I is used, and the exact value $K_I(=A^o_1\sqrt{2\pi a})$ can be obtained. For interface crack in bimaterials, although external traction is symmetric about the x-axis, τ_{xy} exists along the x-axis because the elastic properties are not symmetric about x-axis. Under these circumstances, the coefficients A^o_n and A^*_n must be used.

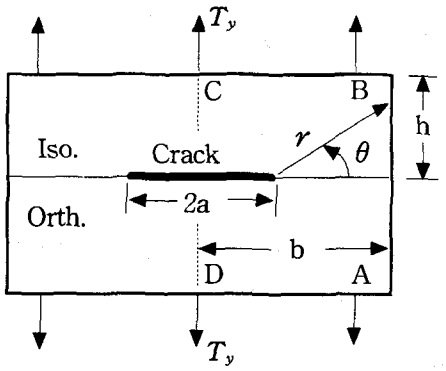

Fig. 1 Model of rectangular isotropic-orthotropic bimaterial plate.

4. Experimental Details and Analysis

The bimaterials used to evaluate the fracture parameters consist of the PSM-1 for isotropic material (Mat.1) and Scotchply-1002 for orthotropic material (Mat.2). The material properties are shown in Table 1. The width, hight and thickness of specimen are 254mm, 508mm and 9.525mm respectively.

Fig. 2 (a) and (b) show the Isochromatic fringe patterns in the PSM for a static center crack in PSM-1/Scotchply-1002 bimaterial. As known, the fringe orders (N=3.5, 4.0, 4.5, 5.0) at crack are greater than when α=90° than when α=0°. The orthotropic material of α=0° is more compliant than that of α=90° for loading direction. Thus, It can be inferred that the stress intensity factor at crack tip of the isotropic material bonded with orthotropic material of α=90° is greater than that bonded with orthotropic material of α=0° under same load.

Fig. 3 (a) and (b) show the Isochromatic fringe patterns in the PSM-1 half for a edge crack propagating along the interface of a PSM-1/Scotchply-1002 bimaterial photoed by Speed Digital Carmer (IMACON-200), with which 16 images of the propagating crack were captured. The stress field equations (1) ~(3) combined with the stress optic law define the order of the isochromatics at any given point. The unknown coefficients in equations (1) ~(3) were extracted from the isochromatics using the non-linear least square method[7].

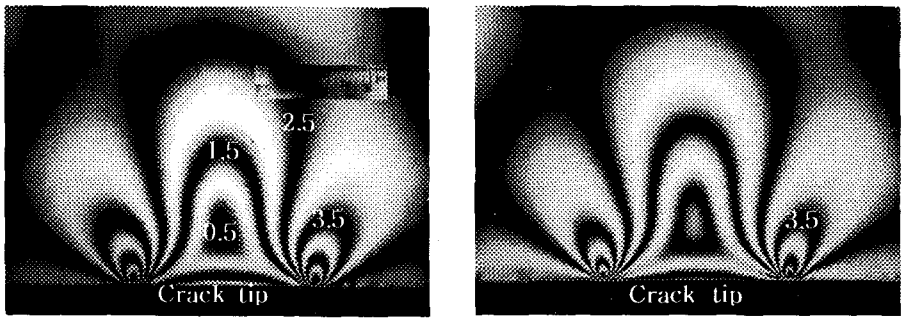

(a) α=90° (b) α=0°

Fig. 2 Isochromatic fringe patterns for a static center crack in PSM/Scotchply bimaterial photoed by Digital Carmer. 2a/W=0.3, Load=3.56KN, W=254mm, H/W=0.3.

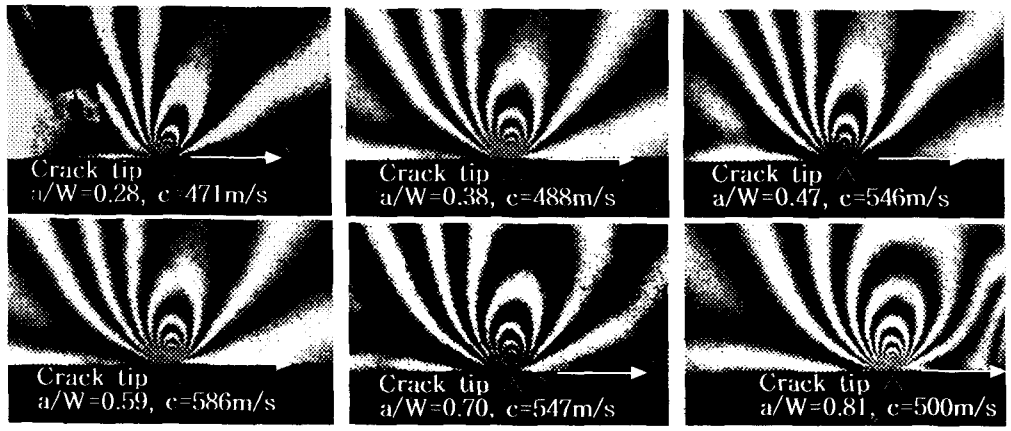

(α=90°)

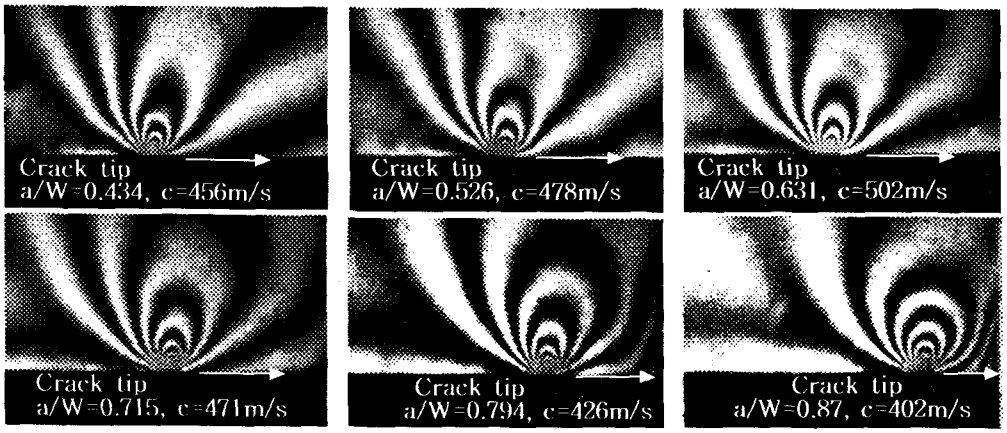

(α=0°)

Fig. 3 Isochromatic fringe patterns for a propagating crack in PSM/Scotchply bimaterial photoed by High-Speed Digital Carmer.

Table 1. Material properties for bimaterials.

Property	PSM		Property	Scotchply	
	Stat.	Dyna.		Stat.	Dyna.
E(GPa)	2.50	2.76	E_L	39.3	47.12
			E_T	9.67	13.05
μ(GPa)	.905	1.0	μ_{LT}	3.10	3.89
ν	.380	.35	ν_{LT}	.254	.254
ρ(Kg/m^3)	1200	1200	ρ	1860	1860
f_σ(KN/m)	6.45	7.0	f_σ	-	-

E : Young's modulus, μ : Shear modulus, ν : Poisson's ratio, ρ : Density, f_σ : Material fringe value, L, T : Fiber direction, Normal to fiber one.

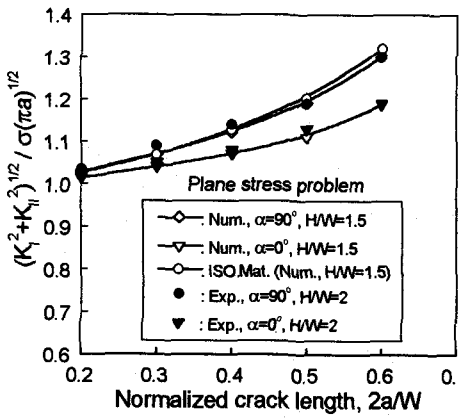

Fig.4 The $\sqrt{K_I^2+K_{II}^2}/\sigma\sqrt{\pi a}$ with normalized crack length for static load.

5. Evaluation of Fracture Parameters

Fig.4 shows the normalized stress intensity factors (NSIFs) obtained from the numerical analysis and the experiments for static crack in PSM-1/Scotchply-1002 bimaterial. The normalized stress intensity factors for α=0° are less than those for α=90° which are very close to those of isotropic material. As the normalized crack length approaches to 0.2, the normalized stress intensity factors approach to 1.0095, which is a good agreement with the results from equation (6) for stationary crack. Generally, the normalized stress intensity factor for embedded cracks aligned normal to fibers is greater than those of crack aligned with fiber[8]. It can be identified that NSIFs for the isotropic-orthotropic bimaterial also show the same tendency as those of orthotropic materials.

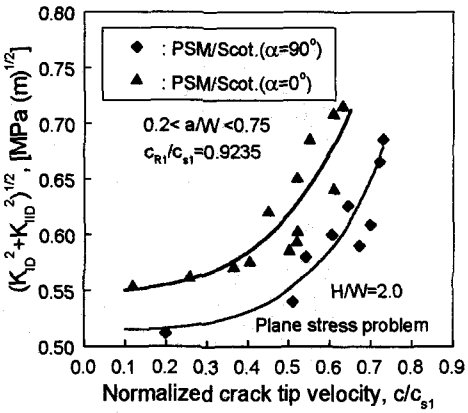

Fig. 5 The $\sqrt{K_{ID}^2+K_{IID}^2}$ with normalized crack length for a propagating crack.

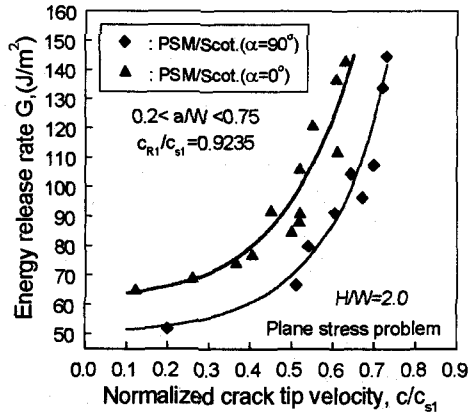

Fig. 6 The energy release rate G with normalized crack length for a propagating crack.

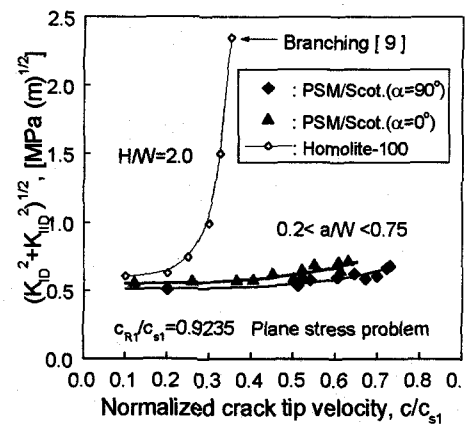

Fig. 7 The dynamic stress intensity factors between an isotropic material and an isotropic-orthotropic bimaterial.

Fig.5 shows the amplitude of dynamic complex stress intensity factor, $|K_D|$, as a function of the normalized crack speed for propagating interfacial crack for both fiber orientations. As opposed to the stationary crack, the $|K_D|$ values are higher when the fibers are aligned parallel to the interface(α=0°).When the fibers are perpendicular to the interface, the ends of the fibers meeting the interface act as weak spots in the path of the propagating crack resulting in smaller values of the $|K_D|$. The $|K_D|$ versus c relationship for bimaterials having high mismatch, proposed by Kavaturu and Shukla[7], indicates that the $|K_D|$ initially increased with crack velocity and then decreases and remains finite as the crack velocity approaches the Rayleigh wave speed of the more compliant material. Especially, the decrease in $|K_D|$ occurs in the velocity range of $0.8< c/c_{s1} <0.9$, under shear dominated crack growth[7]. The $|K_D|$ in the present study registers an increasing trend with increasing crack velocity for the velocity ranges observed. This is could be due to the low mismatch levels (ε=0.07 ~0.14) and opening mode dominated nature of the crack growth. As shown in figure 7, even though the $|K_D|$ vs c relationship is similar to that for isotropic homogeneous materials, the rate of increase of G or $|K_D|$ with crack speed is not as drastic as that reported for homogeneous materials[9]. Hence, further experimental data in the high velocity regime is necessary to confirm this similarity.

The energy release rate G, as a function of normalized crack speed, shown in Fig. 6, also indicate the same trend as the $|K_D|$. The dynamic energy release rate for an isotropic material increases rapidly with crack propagation velocity, and becomes infinite value when a crack velocity approaches the Rayleigh wave speed. It causes the crack to branch at low velocity. But the dynamic energy release rate for an interfacial propagating crack of bimaterial increases slowly with crack propagation velocity, and remains finite for the velocity ranges observed in this study.

6. Conclusions

It is confirmed from numerical and experimental method that the normalized stress intensity factors for static crack is greater when α=90° than when α=0°, and those when α=90° are similar to ones of isotropic material. The dynamic stress intensity factors for interfacial propagating crack are greater when α=0° than α=90°. It can be inferred that the bonding force at interface is greater when α=0° than when α=90°. For the velocity ranges ($0.1< c/c_{s1}<0.7$) observed in this study, the complex dynamic stress intensity factor $|K_D|$ increases with crack speed c, however, the rate of increase of $|K_D|$ with crack speed is not as drastic as that reported for homogeneous materials.

References

(1) Yang, W., Suo, Z. and Shih, C. F., 1991, " Mechanics of Dynamic Debonding", *Proc., R. Soc. of Lond*, A.433, pp.679 ~697.

(2) Deng, X., 1993, "General Crack-Tip Fields for Stationary and Steadily Growing Interface Cracks in Anisotropic Bimaterials", *J. of Appl. Mech.*, Vol. 60, pp.183 ~189.

(3) Lee, K. H., 1999, "Stress and Displacement Fields for Propagating Crack along Interface of Isotropic-Orthotropic Material under Dynamic Mode I and II Load", *KSME Journal (A)*, Vol.23, No.9, pp.1463 ~1475.

(4) Gdoutos, E .E. and Papakaliatakis, 1982 , "Photoelastic Study of a Bimaterial Plate with a Crack Along the Interface", *Engng. Fract. Mech.* Vol. 16, No. 2, pp.177.

(5) Lu, H. and Chiang F. P.,1993, "Photoelastic Determination of Stress Intensity Factor of an Interfacial Crack in a Bi-material",*J. of Appl. Mech.*, Vol. 60, pp.93 ~100.

(6) Lambros J. and Rosakis, A. J., 1995, "Development a Dynamic Decohesion Criterion for Subsonic Fracture of the Interface Between Two Dissimilar Materials", *Proc. R. Soc. Lond.(A)*, 451, pp.711 ~736.

(7) Kavaturu, M. and Shukla, A., 1998, "Dynamic Fracture Criteria for Crack Growth Along Bimaterial Interfaces", *J. of Appl. Mech.*, Vol. 65, pp.293 ~299.

(8) Lee, K. H. and Choi, Y. C., 1999, "Analysis of Propagating Flat Crack in Orthotropic Rectangular Plate", *KSME Journal(A)*, Vol.23, No.1, pp.89 ~98.

(9) Kobayashi, T. and Dally, J. W, 1977, "The relation Between Crack Velocity and Sress Intensity Factor in Birefringent Polymers, Fast Fracture and Crack Arrest", *ASTM STP* 627, pp.257 ~273.